Preparation of Ag/g-C_3N_4/C Ternary Nanocomposites and Study of their Photoreactivity

XIANHUA LI[1], QINGBO YU[2]*, SONGHUI FANG[2] AND XIAOZE WANG[2]

[1]*School of Mechanical Engineering, Anhui University of Science and Technology, Huainan 232001, People's Republic of China.*

[2]*Department of Materials Science and Engineering, Anhui University of Science and Technology, Huainan 232001, People's Republic of China.*

ABSTRACT

In this article, novel Ag/g-C_3N_4/C ternary nanocomposites with leaves-fructification-like architecture were prepared by hydrothermal treatment of the mixture of g-C_3N_4 nanosheets, glucose solution and silver nitrate. In order to comparison, a series of nanomaterials including g-C_3N_4 nanosheets, binary nanocomposites (g-C_3N_4/C) and ternary nanocomposites (Ag/g-C_3N_4/C) loaded with different amounts of carbon were prepared and characterized in detail. The Ag/g-C_3N_4/C1 nanocomposites showed the highest photocatalytic activity towards degradation of MB. The reason for this was bio-inspired structures effects and the synergistic effect of Ag, g-C_3N_4 and carbon, which increased visible-light absorption due to their surface plasmon resonance (SPR) effect of Ag, enhanced adsorption for the MB because of the negatively charged surface of Ag, improved photoinduced electron–hole separation efficiency owing to carbon and bio-inspired structures effects.

KEYWORDS: *Photocatalyst, Ag/g-C_3N_4/C nanocomposites, Structure, Synergistic effect*

1. INTRODUCTION

Sunlight-driven semiconductor photocatalysts have attracted intense attention for solving the growing severity of environment problems and an energy crisis [1, 2]. To the effective utilization of solar energy, considerable studies have been focused on developing inexpensive, earth-abundant, and visible light-driven photocatalyst [3]. Among various semiconductors, graphitic carbon nitride (g-C_3N_4) is indeed an attractive type of visible-light-induced photocatalyst, which showed proper electronic structure (Eg≈2.7 eV), low toxicity, low cost and high chemical and thermal stability [4-6]. However, its photocatalytic efficiency is still limited because of the high recombination of photo-generated carriers and insufficient photon absorption above 450 nm [7].

J. Polym. Mater. Vol. **34,** No. 4, 2017, 681-693

Correspondence author e-mail: yugingbo007@163.com

Deposition of silver (Ag) nanoparticles on the semiconductor photocatalysts has been demonstrated as an effectual method, which can not only inhibit photoinduced charge carrier recombination [8-10], but also enhance the sunlight harvesting of catalysts by a surface plasmon resonance (SPR) effect [11, 12]. A great deal of scientific research proved that g-C_3N_4 with Ag as an active component, showed remarkable visible-light-driven photocatalytic activity [13]. Another widely reported approach to enhance g-C_3N_4's activity is to couple it with other metal-free carbonaceous materials such as graphene [14], carbon nanotubes [15], carbon quantum dots (CQDs) [16]. The carbonaceous materials in g-C_3N_4 can not only utilize the full spectrum of sunlight due to the up-conversion effect, but also separate the electron-hole pairs upon the conjugated π structure. In our previous work, the graphene-containing composites showed elevated activity of g-C_3N_4 on degradation for methylene blue (MB) [14, 17]. Nevertheless, reports on Ag/ g-C_3N_4/C ternary nanocomposite for highly efficient photocatalytic activity remain rare.

One main challenge is to construct the system of Ag, g-C_3N_4 and carbon for further improving the quantum yield and expanding the light absorption. Biomimetics is a splendiferous strategy for scientific and technological problems [18]. Many studies also revealed that photocatalyst with bio-inspired structures show higher photocatalytic activity [19]. Bio-inspired plasmonic nanoarchitectured hybrid system is constructed by yan et al [20]. Experiments show the structural effects on obvious far red-to-NIR photocatalysis enhancement.

Here, we prepared a novel Ag/g-C_3N_4/C ternary composite with leaves-fructification-like architecture by hydrothermal treatment. The chemical compositions, structures and morphologies were fully characterized.

2. EXPERIMENTAL

2.1 Materials

Dicyandiamide (DCD), glucose, potassium dichromate ($K_2Cr_2O_7$), silver nitrate ($AgNO_3$), concentrated sulfuric acid (H_2SO_4) and potassium persulfate ($K_2S_2O_8$) were purchased from Fuchen Chemical Reagent Co. (Tianjin, China). All other chemicals were used as received without further purification.

2.2 Preparation of g-C_3N_4 nanosheets and g-C_3N_4/C nanocomposites

The g-C_3N_4 nanosheets used in our experiments were prepared by the previously reported literature [21]. The g-C_3N_4/C nanocomposites were carried out as follows: At first, 3.3 g glucose was dissolved in 22 mL water to obtain a clear solution. Then, 10 mL g-C_3N_4 nanosheets (3 mg/mL) were added. After ultrasonic treatment, the resulting slurry was transferred into a Teflon-lined autoclave and maintained at 180°C for 10 h, and then cooled to ambient temperature. The obtained products were collected, washed, finally dried, and named as g-C_3N_4/C1. The composites with different residence time (6 h and 8 h) were prepared in similar procedure and named as g-C_3N_4/C3 and g-C_3N_4/C2, respectively.

2.3 Preparation of Ag/g-C_3N_4/C nanocomposites

The preparation of Ag/g-C_3N_4/C nanocomposites is similar to g-C_3N_4/C nanocomposites. The difference is the addition of $AgNO_3$ (30 mL, 0.3 mg/mL) in slurry of glucose solution and g-C_3N_4 nanosheets. The obtained products were named as Ag/g-C_3N_4/C1, Ag/g-C_3N_4/C2 and Ag/g-C_3N_4/C3 according to the different residence time (6 h, 8 h and 10 h).

2.4 Characterizations

The crystal structures of the samples were characterized on a XD-3 X-ray diffractometer. The morphologies and microstructures of the as-prepared samples were obtained on a S4800 ESEM FEG scanning electron mi-

croscope. Fourier transform infrared (FTIR) spectra were measured with NEXUS-870 spectrophotometer. X-ray photoelectron spectroscopy (XPS) measurements were recorded with a VGESCALAB MKII X-ray photoelectron spectrometer. UV-vis (L98,L176,L192) spectra were recorded on U-4100UV spectrophotometer. Photocurrent measurements were measured with an electrochemical analyzer (CHI660E, CHI Shanghai, Inc.) by using three-electrode cells.

2.5 Evaluation of the photocatalytic activity

The MB was used as a probe molecule. The adsorption capacity (C, μmol/g) of the as-prepared samples was calculated by Eq. (1).

$$C = \frac{I_0 - I_2}{I_0} \times \frac{C_0 \times V}{m} \quad (1)$$

where C_0 is the initial concentration of MB (2.7×10^{-5}mol/L), I_0 is the initial absorbance of MB, V is the solution volume of MB (50 mL), I_2 is the absorbance after stirring for 2 h, and m is the mass of the as-prepared samples (25 mg).

After the absorption of MB, A 300 W Xe lamp equipped with a 420 nm cut off filter was used as light source. The decreases of MB concentrations were measured by a UV-vis spectrophotometer at 664 nm with regular intervals. In detail, 25 mg sample was dispersed in MB (2.7×10^{-5} mol/L) aqueous solution. After saturated MB adsorption, the 3 ml liquid were collected at the predetermined irradiation time. The MB concentrations were monitored using a UV-vis spectrophotometer. The stability of the photocatalyst also was performed, that is, the obtained photocatalyst by a vacuum filter was redispersed in MB solution. The photocatalytic process was the same as the above.

3. Results and Discussion

3.1 Morphology and structure characterization

The SEM image shown in Fig. 1a demonstrates that the as-prepared nanosheets by chemical oxidation have independent lamellar structure. The XRD pattern (Fig. 1b) confirms the nanosheets belong to g-C_3N_4.

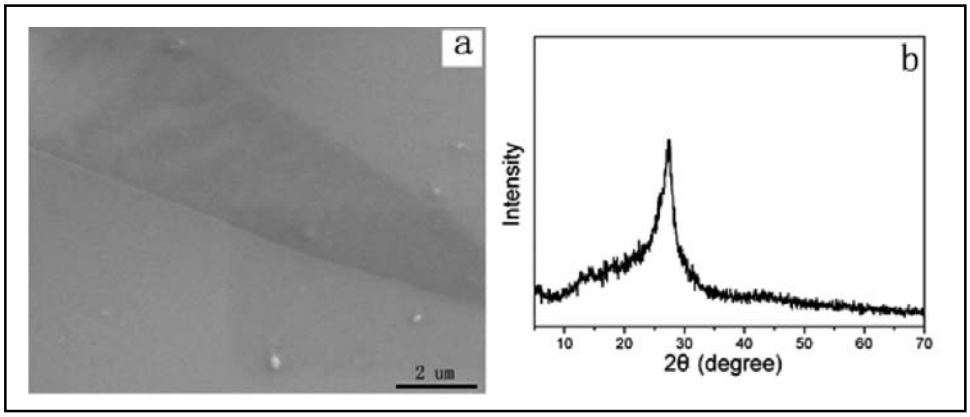

Fig. 1 SEM image (a) and XRD pattern (b) of g-C_3N_4 nanosheets.

After hydrothermal treatment of the mixture of g-C_3N_4 nanosheets and glucose solution, the morphology and microstructure of the nanocomposite were characterized. XRD pattern of the g-C_3N_4/C1 nanocomposites (Fig 2a-2) displays a broad diffraction peak in 2 theta ranging from 16.6° to 29.2° , which is analogous to carbon's spectra (Fig 2a-1). It is noted that

no diffraction peaks of g-C_3N_4 nanosheets can be observed in nanocomposite, maybe due to the small amount of g-C_3N_4 nanosheets used and/or due to the hide by the diffraction peak of carbon. FTIR spectra were employed to further dissect the nanocomposites (Fig. 2b). It can be observed that the neat carbon shows obvious peaks at 2920 cm^{-1} and 2842 cm^{-1}, corresponding to the characteristic stretching vibrations of carbonyl C–H and C=O [22]. The peak at 1627 cm^{-1} are attributed to aromatic C=C vibrations [23, 24]. The g-C_3N_4/C1 nanocomposites and pure g-C_3N_4 nanosheets display similar spectra, suggesting the introduction of carbon does not change the chemical structure of the g-C_3N_4 nanosheets. The XPS measurement in Fig. 2c shows that g-C_3N_4/C1 nanocomposites are mainly composed of C, N and O. The high resolution XPS spectra of C1s are provided in Fig 2d. Two peaks at 288.4 eV and 284.9 eV are attributed to the N-C=N backbone of the g-C_3N_4 and surface adventitious carbon, respectively [25]. The C1s spectrum is similar to that of pure g-C_3N_4 nanosheets. However, the C/N ration of g-C_3N_4/C1 nanocomposites calculated using XPS is 0.89, a little higher in comparison with the value 0.71 in g-C_3N_4 nanosheets, suggesting a high concentration of C in g-C_3N_4/C1 nanocomposites. Combined with the FTIR and XRD analysis, it can be known that the g-C_3N_4/C1 nanocomposite is obtained.

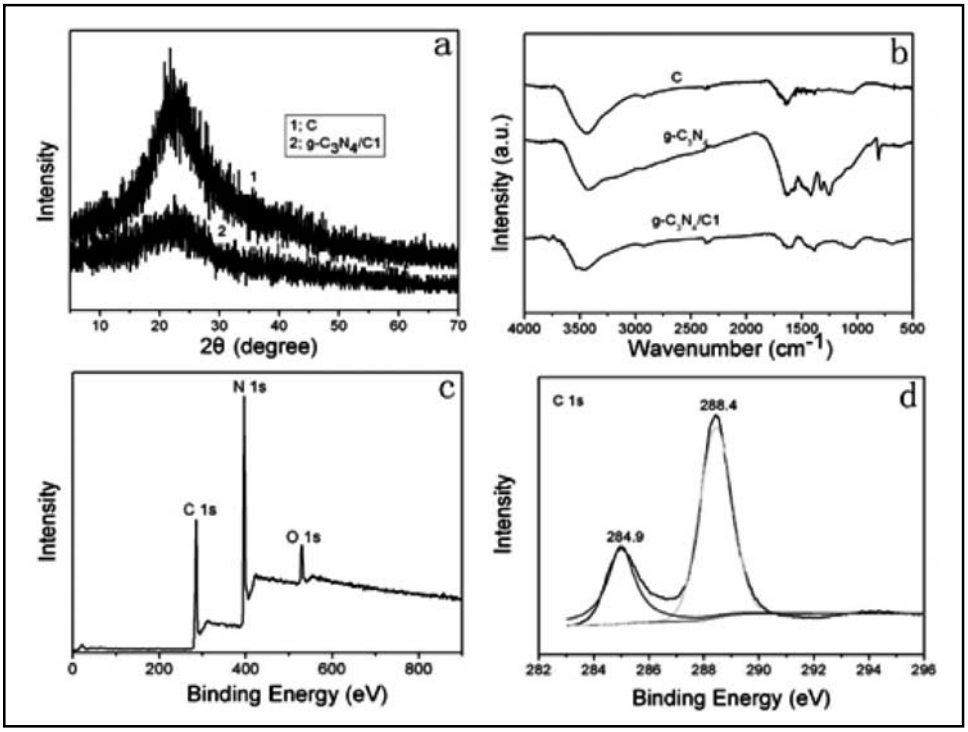

Fig. 2. XRD patterns (a) and FTIR spectra (b) of samples; XPS spectra of g-C_3N_4/C1 nanocomposite: (c) Survey spectrum, (d) C 1s peak.

As shown in Fig. 3a and b, the g-C_3N_4/C1 nanocomposite was made up of nanospheres and flocculent material. The flocculent material is similar to pine leaves, and the nanospheres is similar to fructification in pine (Fig. 3e). The whole leaves-fructification-like architecture may be beneficial to the performance of the product due to the bio-inspired structures effects. Mother Nature has already known to use the wide spectrum and improve the photosynthesis. Spinner et al found that snake skins are able for NIR harvesting due to the nanoarchitecture [26]. Up to now, most efforts are focused on preparation of biomimetic material. Fu et al fabricate a novel leaf-like CdS micro-/nanostructure, which exhibited a fascinating performance in gas sensor [27]. So the leaves-fructification-like architecture may be to develop the photocatalyst properties of the g-C_3N_4/C1 nanocomposite. Aside from the nanoarchitecture, it is noteworthy that the morphology of the g-C_3N_4/C1 nanocomposites is completely different from the g-C_3N_4 nanosheets' (Fig. 1a), indicating that the addition of carbon has tremendous influence on the microstructures. It also can be seen that the surface of nanocomposite is smooth (Fig. 3b). A series of experiments were performed by varying the reaction time, while keeping other parameters constant. For g-C_3N_4/C2 and g-C_3N_4/C3, the number of nanospheres decreases with decrease in the reaction time (Fig. 3c, d). The element ratio of C to N for g-C_3N_4/C nanocomposite also steady decreases from 0.85 (g-C_3N_4/C2) to 0.80 (g-C_3N_4/C3) showed by element analysis, which may be influence the performance of the subsequent photodegradation of dye [12].

After hydrothermal treatment of the mixture of g-C_3N_4 nanosheets, glucose solution and $AgNO_3$, the Ag/g-C_3N_4/C1 nanocomposites were also made up of nanospheres and flocculent material (Fig. 4a and b), which is similar the g-C_3N_4/C3 nanocomposite with leaves-fructification-like architecture. However, the nanospheres in ternary nanocomposites were more uniformly distributed (comparing 4a with 3a), and the flocculent material was filled between nanospheres. It is noteworthy that the surface of ternary nanocomposite is relative rough in Fig. 4b compared with Fig. 3b. The XRD pattern shown in Fig. 4c is the same as that of the g-C_3N_4/C1 nanocomposites (Fig. 2a-2) except the presence of the (111), (200), (220) and (311) planes of face centered cubic (FCC) of metallic Ag (JCPDS card no. 65-2871). Furthermore, it could be clearly seen that the main characteistic peaks of Ag/g-C_3N_4/C1 nanocomposites in FTIR spectra (Fig. 4d) is similar the g-C_3N_4/C1 nanocomposites (Fig. 2b), suggesting that no structural change of binary nanocomposites occurs during the introduction of Ag. All these analyses confirm as-obtained ternary nanocomposites are Ag/g-C_3N_4/C1 nanocomposites consisting of pine leaves-fructification architecture covering Ag.

With increase in the hydrothermal treatment duration (8 h and 10 h), the morphologies of the resultant products (Fig. 5a and b) are similar to one that treated during shorter time (6 h). However, the broad diffraction peak in 2 theta ranging from 16.6° to 29.2° become weaker gradually with increasing hydrothermal treatment duration (Fig. 5c and d), suggesting that plasmonic metal (Ag) have been successfully deposited onto the surface of g-C_3N_4/C nanocomposites [28].

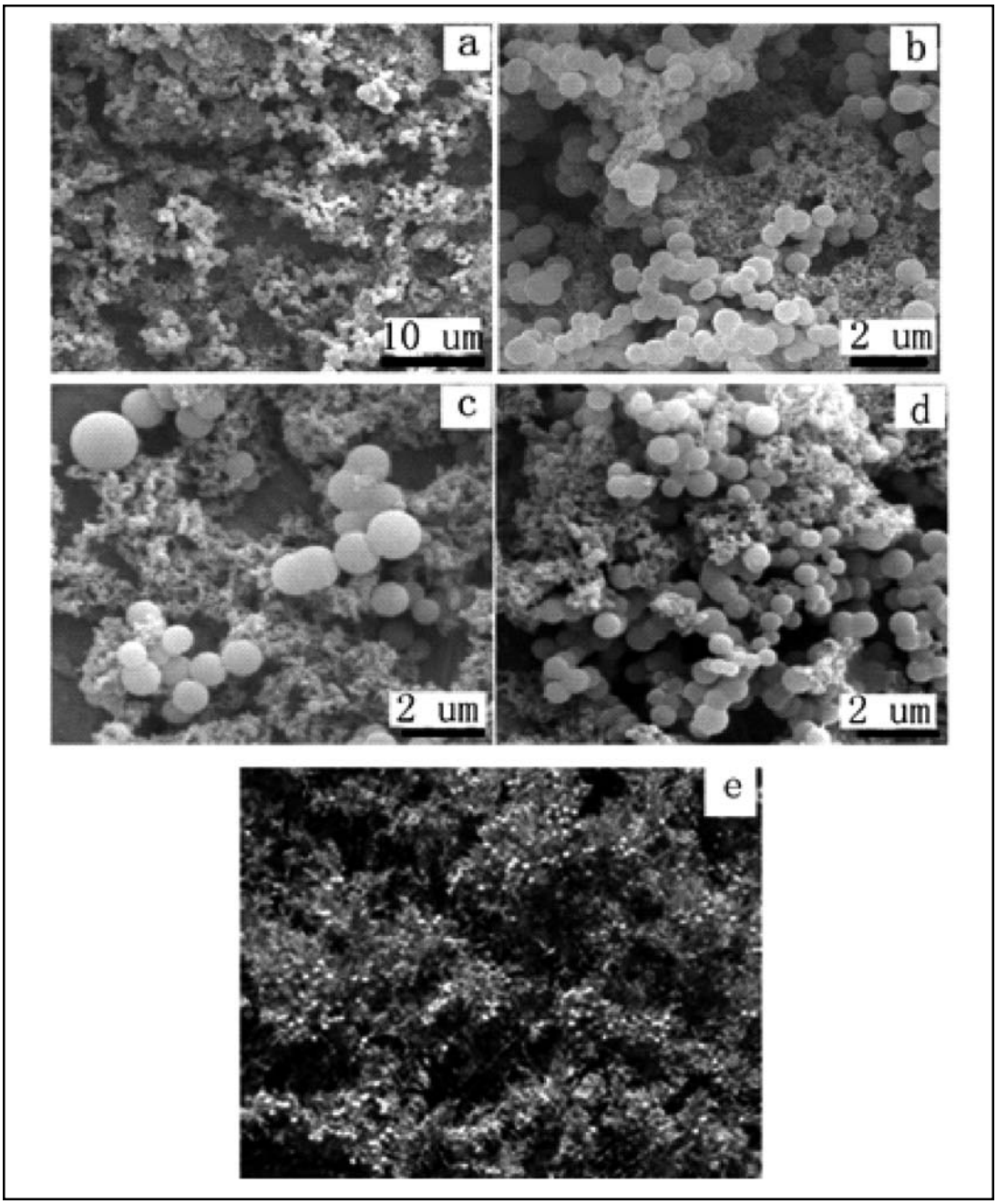

Fig. 3. SEM images of the g-C_3N_4/C1 (a, b) with different magnifications, g-C_3N_4/C3 (c), g-C_3N_4/C2 (d); Photograph (e) of the pine leaves and fructification.

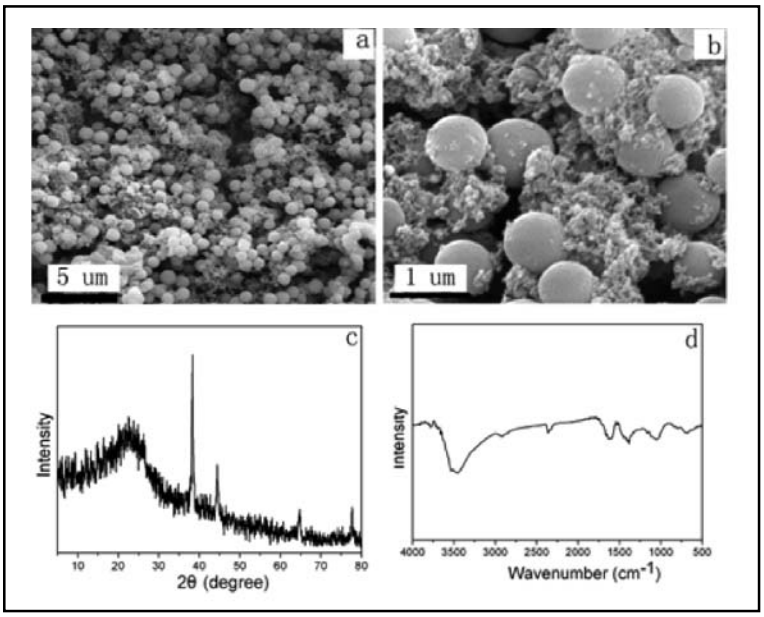

Fig. 4. SEM images (a, b) with different magnifications, XRD pattern (c) and FTIR spectra (d) of Ag/g-C_3N_4/C1.

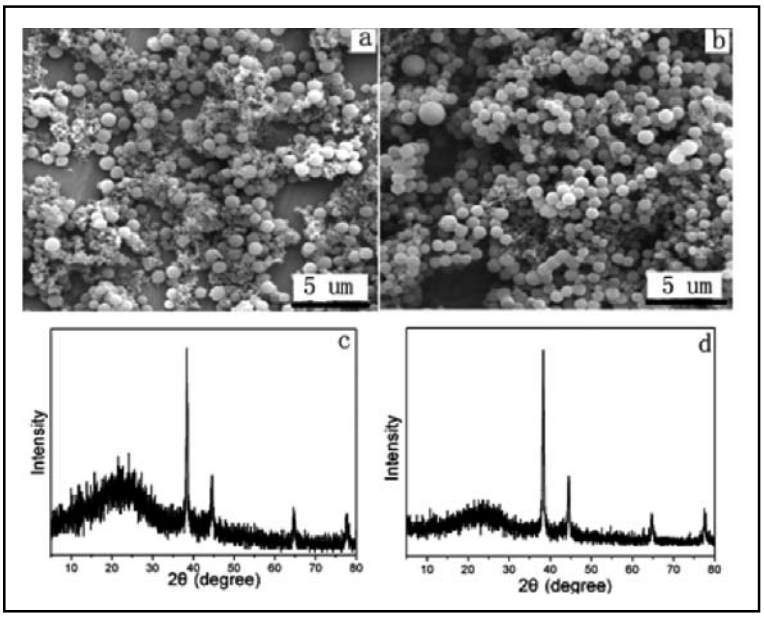

Fig. 5. SEM images (a, b) and XRD patterns (c, d) of Ag/g-C_3N_4/C2 (a, c) and Ag/g-C_3N_4/C3 (b, d).

Fig. 6 shows the UV-vis absorption spectra of the different samples. The pure g-C_3N_4 nanosheets have the absorption edge at about 480 nm (Fig. 6a), which is assigned to band gap absorption (2.7 eV) [29]. The g-C_3N_4/C3 nanocomposites enhances its light absorption over the whole range of wavelengths investigated (Fig. 6a), due to the strong absorption of carbon in the visible light region [14]. While the Ag/g-C_3N_4/C1 nanocomposites presents a weak absorption in the range of 450-650 nm (Fig. 6a), which results from the localized surface plasmon resonance (LSPR) of Ag loaded in the nanocomposites. Meanwhile, the g-C_3N_4/C nanocomposites show weaker absorption with increasing the reaction time, namely increasing carbon content (Fig. 6b), due to bio-inspired structures effects. However, the Ag/g-C_3N_4/C nanocomposites show stronger absorption with increasing the reaction time (Fig. 6b), and the LSPR peaks broaden obviously because the Ag nanoparticles have a wide particle size distribution [12]. All these analyses reveal that the proper proportion of Ag, g-C_3N_4 nanosheets and carbon influence the light absorption of the resultant products.

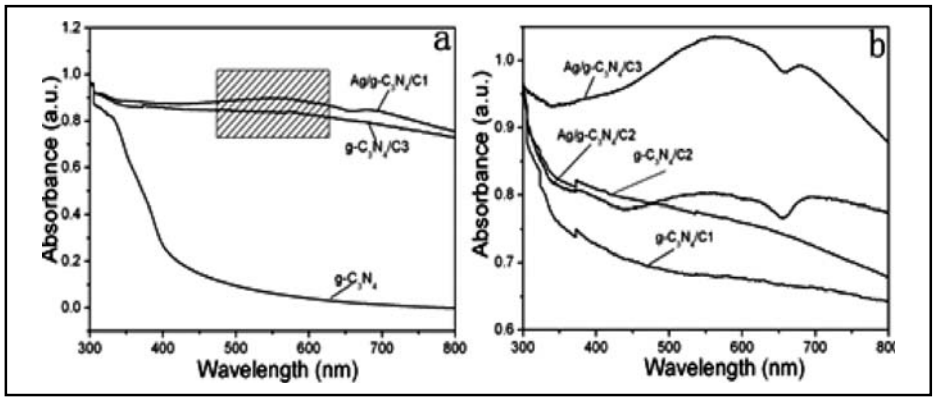

Fig. 6. UV-vis absorption of the different samples.

3.2 Adsorption and photocatalytic degradation of MB

It is well known that the high adsorption capability of the catalyst is important and can make the catalyst behave as a collector to gather the dye without sunlight [30]. In addition, the adsorption of the dye is important for efficient dye-photosensitisation, enhancing photodegradation reactions [31]. As shown in Fig. 7, the adsorption capability of pure g-C_3N_4 nanosheets is about 60 μmol/g. The g-C_3N_4/C nanocomposites have approximate adsorption capacities. However, the ternary nanocomposites from Ag/g-C_3N_4/C1 to Ag/g-C_3N_4/C3 possess high adsorption capacity to the cationic dye of methylene blue (MB). The Zeta potential of the Ag colloid is tested to be -44 mV [32], which may play a key role in the removal of cationic dye (MB). The integration of high adsorption capacity and the photocatalytic nature of g-C_3N_4 nanosheets will endow the g-C_3N_4-containing nanocomposites a strong candidate for subsequent photodegradation of MB.

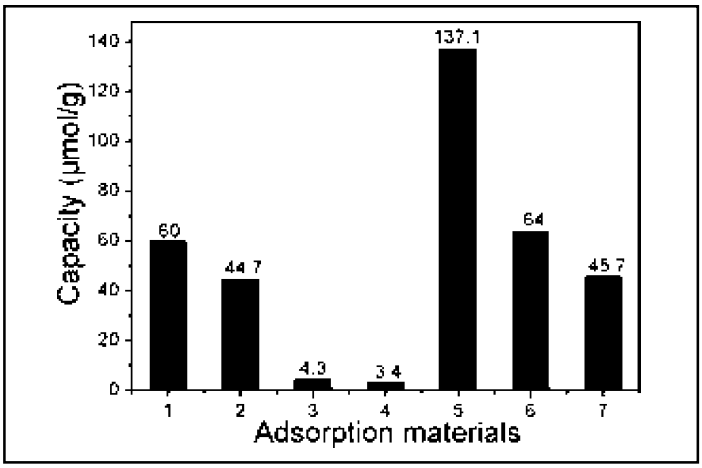

Fig. 7. The adsorption of g-C_3N_4 (1), g-C_3N_4/C3 (2), g-C_3N_4/C2 (3), g-C_3N_4/C1 (4), Ag/ g-C_3N_4/C1 (5), Ag/ g-C_3N_4/C2 (6), Ag/ g-C_3N_4/C3 (7).

After the absorption balance in MB, the photocatalytic performance of these catalysts was examined, and the results are summarized in Fig.8. In the presence of pure g-C_3N_4 nanosheets, the degradation of MB is 47% after 40 min of illumination (Fig. 8a). The g-C_3N_4 nanosheets compounded with carbon exhibit higher photocatalytic performance due to the bio-inspired structures effects (Fig. 8a). It is noteworthy that the photocatalytic efficiency can be further improved by introducing Ag in the nanocomposites. 75% of MB was photodegraded over the Ag/g-C_3N_4/C tannery nanocomposites after 40 min of illumination (Fig. 8a). The plot of the irradiation time (t) against $\ln(C_0/C_t)$ is shown in Fig. 8b, which is linear. The reaction constant κ of the ternary nanocomposites (Ag g-C_3N_4/C) is the biggest, suggesting the highest photocatalytic activity towards degradation of MB. The enhanced photocatalytic activity of the ternary nanocomposites contributed to bio-inspired structures effects, the synergistic effect of the three components and the dye-sensitisation caused by stronger adsorption in MB. To the leaves-fructification-like architecture, the Ag/g-C_3N_4/C tannery nanocomposites benefit the transfer of photogenerated electrons using the channel between nanospheres (fructification) and flocculent material (leaves). To the synergistic effect of the three components, the photogenerated electron-hole was formed by the excitations of both the band-gap transition of g-C_3N_4 nanosheets and the surface plasmon resonance (SPR) of metal Ag after irradiating with visible light. The SPR properties of Ag can enhance the visible light harvesting. The carbon can rapidly transfer the photogenerated electrons, and obtain an efficient charge separation [33]. To the dye-sensitisation, some pioneering endeavors discovered that the adsorption of dye is an important factor [31]. Both the g-C_3N_4 nanosheets and the metal (Ag) provide high adsorption to MB molecules, which can enhance photodegradation under visible light.

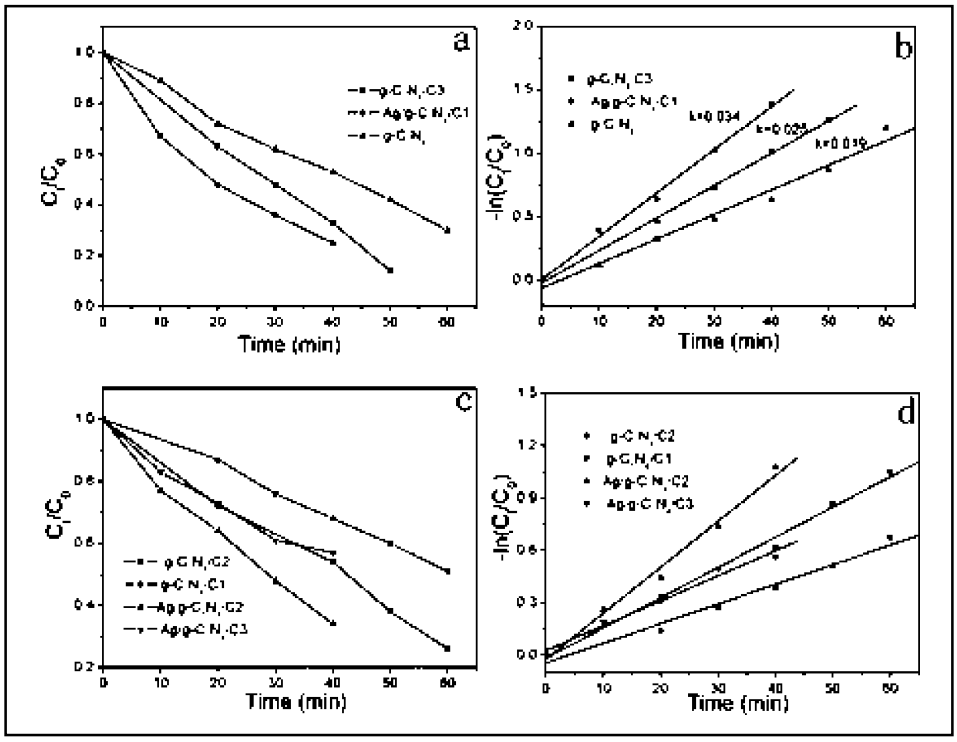

Fig. 8. Photocatalytic degradation of MB (a, c) and the kinetic linear simulation curves (b, d) of as-prepared samples.

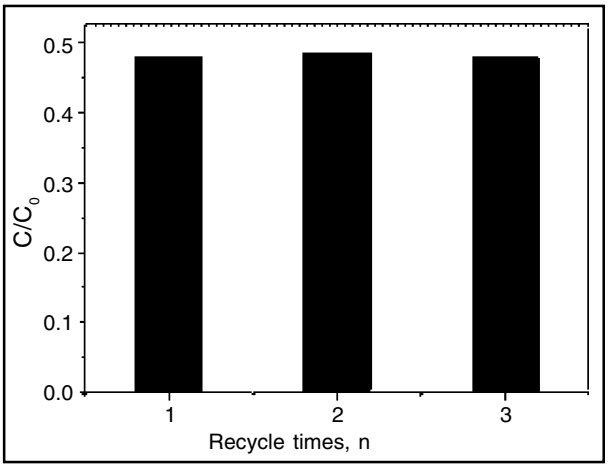

Fig. 9 The stability of the Ag/g-C_3N_4/C1 after three cycles.

All of these effects from the three components, bio-inspired structures and dye-sensitisation enhanced the photocatalytic activity of Ag/g-C_3N_4/C nanocomposites.

As shown in Fig 8 c and d, further increasing the element ratio of C to N no matter in binary nanocomposites (g-C_3N_4/C1, g-C_3N_4/C2) or in corresponding ternary nanocomposites (Ag/g-C_3N_4/C2, Ag/g-C_3N_4/C3), the photocatalytic activity decreased. The decrease in the samples with a heavy loading carbon is maybe due to the shading effect (Fig 6b) and the gradual fall in adsorption to MB molecules (Fig. 7). Thus, excess compounded with carbon is not favorable for the improving photocatalytic activity. Fig. 9 shows that the Ag/g-C_3N_4/C1 is stable for each cycle. The MB decomposed during the 20 min irradiation, have a small decline after three cycles.

3.3 Photoelectrochemical measurements

The transient photocurrent responses of g-C_3N_4 nanosheets, g-C_3N_4/C3 nanocomposites and Ag/g-C_3N_4/C1 nanocomposites were investigated in Fig. 10. The photocurrent of g-C_3N_4 nanosheets is very low (1.44 μA/cm^2). After introducing carbon, the photocurrent is improved (3.72 μA/cm^2). The ternary nanocomposites of Ag/g-C_3N_4/C1 show the strongest photocurrent response, which increase to 5.88 μA/cm^2. The result is consistent with the photocatalytic performance, confirming that the Ag/g-C_3N_4/C1 ternary nanocomposites possess the highest visible light conversion efficiency, due to the synergistic effect of Ag, g-C_3N_4, and carbon.

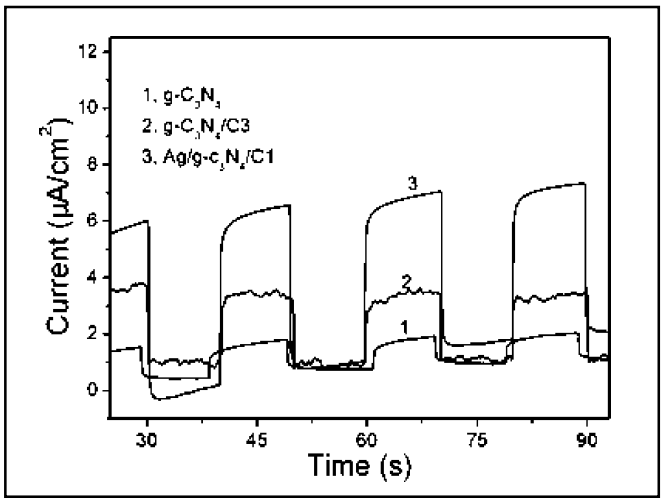

Fig. 10. I-t curves of the samples.

4. Conclusions

In summary, we reported a facile method on fabrication Ag/g-C_3N_4/C ternary nanocomposites by hydrothermal treatment with a mixture of g-C_3N_4 nanosheets, glucose solution and $AgNO_3$. In order to comparison, a series of nanomaterials including g-C_3N_4 nanosheets, binary nanocomposites (g-C_3N_4/C1, g-C_3N_4/C2,

g-C_3N_4/C3) and ternary nanocomposites (Ag/g-C_3N_4/C1, Ag/g-C_3N_4/C2, Ag/g-C_3N_4/C3) with different element ratio of C to N were prepared and characterized. The Ag/g-C_3N_4/C1 nanocomposites with leaves-fructification-like architecture showed the highest photocatalytic activity towards degradation of MB. The reason for this was bio-inspired structures effects, the synergistic effect of Ag, g-C_3N_4 and carbon and dye-sensitisation, which increased visible-light absorption, enhanced adsorption for the MB and improved photoinduced electron–hole separation efficiency. So the integration of the three components with leaves-fructification-like architecture can greatly improve the efficiency conversion in visible-light, and improve photocatalytic activity.

Acknowledgements

This work is supported by Postdoctoral Science Foundation of China (2015M571913), and the National Nature Science Foundation of China (21401001).

REFERENCES

1. L. Shao, D. Jiang, P. Xiao, L. Zhu, S. Meng and M. Chen, *Appl. Catal. B-Environ.,* **198** (2016) 200.
2. X. Xiao, J. Wei, Y. Yang, R. Xiong, C. Pan, and J. Shi, *ACS Sustainable Chem. Eng.*, **4** (2016) 3017.
3. S.J. Moniz, S.A. Shevlin, D.J. Martin, Z.X. Guo and J. Tang, *Energy Environ. Sci.*, **8** (2015) 731.
4. S. Yang, Y. Gong, J. Zhang, L. Zhan, L. Ma, Z. Fang, R. Vajtai, X. Wang, P.M. Ajayan, *Adv. Mater.*, **25** (2013) 2452.
5. J. Ding, L. Wang, Q. Liu, Y. Chai, X. Liu, W.-L. Dai, *Appl. Catal. B: Environ.*, **176–177** (2015) 91.
6. X.C. Wang, K. Maeda, A. Thomas, K. Takanabe, G. Xin, J.M. Carlsson, K. Domen and M. Antonietti, *Nat. Mater.,* **8** (2009) 76-80.
7. J. Liu, Y. Liu, N.Y. Liu, Y.Z. Han, X. Zhang, H. Huang, Y. Lifshitz, S.T. Lee, J. Zhong, and Z.H. Kang, *Science*, **347** (2015) 970.
8. T.J. Chen, W. Quan, L.B. Yu, Y.Z. Hong, C.J. Song, M.S. Fan, L.S. Xiao, W. Gu and W.D. Shi, *J. Alloy. Compd.,* **686** (2016) 628.
9. Q.P. Lu, Z.D. Lu, Y.Z. Lu, L.F. Lv, Y. Ning, H.X. Yu, Y.B. Hou, and Y.D. Yin, *Nano Lett.,* **13** (2013) 5698.
10. T. Wang, R. Lv, P. Zhang, C.J. Li, J.L. Gong, *Nanoscale*, **7** (2015) 77.
11. J. Jin, Q.A. Liang, C.Y. Ding, Z.Y. Li and S Xu, *J. Alloy. Compd.*, **691** (2017) 763.
12. B. Li, X. Shao, T. Liu, L. Shao and B. Zhang, B., *Appl. Catal. B-Environ.,* **198** (2016) 325.
13. k. Tian, w.j. Liu and h. Jiang, H., *ACS Sustainable Chem. Eng.,* **3** (2015) 269.
14. Q. Yu, S. Guo, X. Li and M. Zhang, *Mater. Technol.,* **29** (2014) 172.
15. R.C. Pawar, S. Kang, S.H. Ahn and C.S. Lee, *RSC Adv.*, **5** (2015) 24281.
16. K. Li, F. Su and W. Zhang, *Appl. Surf. Sci.,* **375** (2016) 110.
17. Q. Yu, S. Guo, X. Li, X. and M. Zhang*, Russ. J. Phy. Chem. A+.,* **88** (2014) 1643.
18. G.H. Zhang, T.Y. Zhang, B. Li, X. Zhang and X.W. Chen, *Alloy. Compd.,* **668** (2016) 113.
19. L.G. Gao, Y.W. Wang, Y. Yan, Q. Li, C. Hao and T.L. Ma, *J. Colloid Interf. SCI.,* **470** (2016) 10.
20. R. Yan, M. Chen, H. Zhou, T. Liu, X. Tang, K. Zhang, H. Zhu, J. Ye, D. Zhang and T. Fan, *Sci. Rep-uk.,* **6** (2016) 1.
21. H. Jun, B. Sun, L. Sui, D. Qian, M. Chen, *Phys. Chem. Chem. Phys.,* **17** (2015) 3309.
22. M .Sevilla and B. Antonio, *Chem. Eur. J.,* **15** (2009) 4195.
23. B. Hu, S.H. Yu, K. Wang, L. Liu and X.W. Xu, *Dalton Trans.*, **40** (2008) 5414.
24. J. Wang, L. Shi, Y. Gao, H.P. Yang and X.H. Wang, *Transactions of the CSAE.,* **29** (2013) 191.

25. Fang, S., Xia, Y., Lv, K., Li, Q., Sun, J.and Li, M., *Appl. Catal. B-Environ,.***185** (2016) 225.

26. S. Marlene, K. Alexander, N.G. Stanislav and W. Guido, *Sci. Rep.,* **3** (2013) 1846.

27. X. Fu, J. Liu, Y. Wan, X. Zhang, F. Meng and J. Liu, *J. Mater. Chem.,* **22** (2012) 17782.

28. Z. Jiang and J. Xie, *RSC Adv.,* **6** (2016) 3186.

29. S.C. Yan, S.B. Lv, Z.S. Li and Z.G. Zou, *DaltonTrans*., **39** (2010) 1488.

30. X.B. Cao, Z.F. Lu, L.W. Zhu, L. Yang, L. Gu and L.L. Cai, *Nanoscale.,* **6** (2014) 1434.

31. J. Moon, C.Y. Yun, K. Chung, M. Kang and J. Yi, *Catal. Today.,* **87** (2003) 77.

32. M. Muniz-Miranda, S. Caporali, P. Marsili and E. Giorgetti, *Mater. Chem. Phys.,* **167** (2015) 188.

33. Y.J. Wang, R. Shi, J. Lin and Y.F. Zhu, *Appl. Catal. B-Environ,* **100** (2010) 179.

Received: 30-03-2017

Accepted: 31-08-2017